Channels 5:2, 148-160; March/April 2011; © 2011 Landes Bioscience

The elusive role of the SPRY2 domain in RyR1

HanShen Tae,[1,†] Lan Wei,[2,†] Hermia Willemse,[3] Shamaruh Mirza,[3] Esther M. Gallant,[3] Philip G. Board,[3] Robert T. Dirksen,[2,‡] Marco G. Casarotto[3,‡] and Angela F. Dulhunty[3,‡,*]

[1]Howard Florey Institute; University of Melbourne; Parkville, VIC Australia; [2]Department of Pharmacology and Physiology; University of Rochester; Rochester, NY USA; [3]John Curtin School of Medical Research; Australian National University; Canberra, ACT Australia

[†]These authors contributed equally to this work.

[‡]These senior authors contributed equally to this work.

Key words: SPRY domain in RyR1, single RyR1 channel activity, alternatively spliced residues, skeletal muscle, excitation-contraction coupling

Abbreviations: ASI, alternatively spliced region 1 in RyR1-D^{3483}-G^{3487}; ASI/basic region, RyR1 residues-T^{3471}-G^{3500}; ANOVA, analysis of variance; DHPR, dihydropyridine receptor; DHPR II-III loop, loop between the second and third membrane spanning repeat of the DHPR; EC coupling, excitation-contraction coupling; F loop, RyR1 residues P^{1107}-A^{1121} within the SPRY2 domain; γ-GCT, γ-glutamylcyclotransferase; IpTxA, imperatoxin A; PCR, polymerase chain reaction; P_o, open probability; RyR1, type 1 ryanodine receptor; SEM, standard error of the mean; SR, sarcoplasmic reticulum; SPRY, structural domain first identified in *Dictyostelium discoideum* tyrosine kinase spore lysis A (**Spl**A) and the mammalian **Ry**R; SPRY2 domain, the second of three SPRY domains in RyR1- residues S^{1085}-V^{1208}; WT, wild-type; T_o, mean open time; T_c, mean closed time

The second of three SPRY domains (SPRY2, S^{1085}-V^{1208}) located in the skeletal muscle ryanodine receptor (RyR1) is contained within regions of RyR1 that influence EC coupling and bind to imperatoxin A, a toxin probe of RyR1 channel gating. We examined the binding of the **F** loop (P^{1107}-A^{1121}) in SPRY2 to the ASI/basic region in RyR1 (T^{3471}-G^{3500}, containing both alternatively spliced (ASI) residues and neighboring basic amino acids). We then investigated the possible influence of this interaction on excitation contraction (EC) coupling. A peptide with the **F** loop sequence and an antibody to the SPRY2 domain each enhanced RyR1 activity at low concentrations and inhibited at higher concentrations. A peptide containing the ASI/basic sequence bound to SPRY2 and binding decreased ~10-fold following mutation or structural disruption of the basic residues. Binding was abolished by mutation of three critical acidic **F** loop residues. Together these results suggest that the ASI/basic and SPRY2 domains interact in an **F** loop regulatory module. Although a region that includes the SPRY2 domain influences EC coupling, as does the ASI/basic region, Ca^{2+} release during ligand- and depolarization-induced RyR1 activation were not altered by mutation of the three critical **F** loop residues following expression of mutant RyR1 in RyR1-null myotubes. Therefore the electrostatic regulatory interaction between the SPRY2 **F** loop residues (that bind to imperatoxin A) and the ASI/basic residues of RyR1 does not influence bi-directional DHPR-RyR1 signaling during skeletal EC coupling, possibly because the interaction is interrupted by the influence of factors present in intact muscle cells.

Introduction

The Ca^{2+} release channel in the sarcoplasmic reticulum (SR) of skeletal muscle is the type 1 ryanodine receptor (RyR1). The in vivo function of RyR1 in skeletal muscle excitation-contraction (EC) coupling requires the physical presence of the skeletal muscle isoform of the dihydropyridine receptor (DHPR), and more specifically, the II-III loop of its α_{1S} subunit.[1] RyR1 is composed of numerous structural domains, including three "SPRY" domains in the N-terminal 1/3 of each of its four subunits. These domains were named SPRY because they were identified in both *Dictyostelium discoideum* tyrosine kinase spore lysis A (**Spl**A) and the mammalian **Ry**R.[2] The domains generally function as protein-protein interaction motifs and contain two antiparallel β-sheets with β-strands separated by unstructured or α-helical linkers.[3] The three SPRY domains in the RyR are conserved across species from insects to mammals, but their function is unknown. The second of the three domains in RyR1 (SPRY2, S^{1085}-V^{1208}), may function in EC coupling because it overlaps with larger sequences that support skeletal muscle EC coupling[4] and is an in vitro binding partner for both N-terminal residues in the II-III loop of the skeletal muscle DHPR, as well as for the scorpion toxins imperatoxin A (IpTxA) and maurocalcine.[5,6] IpTxA, maurocalcine and the N-terminal part of the II-III loop are used as in vitro probes of RyR1 function.[7-12] All or part of the SPRY2 domain is common to each of the sequences implicated

*Correspondence to: Angela F. Dulhunty; Email: angela.dulhunty@anu.edu.au
Submitted: 05/25/10; Revised: 12/05/10; Accepted: 12/06/10
DOI: 10.4161/chan.5.2.14407

in II-III loop and toxin binding and, since we previously found that the II-III loop and IpTxA interact with the isolated SPRY2 domain,[3,13,14] it is likely that their interaction with SPRY2 underlies the effects of the peptides on RyR channel gating.

Both the conservation of the SPRY2 sequence across species and the likelihood that both IpTxA and the N-terminus of the II-III loop produce significant changes in RyR1 gating by binding to the SPRY2 domain suggest that the SPRY2 domain regulates in vitro RyR1 channel gating. Since the binding of both compounds to the SPRY2 domain increases channel activity, it is possible that the SPRY2 domain contributes to an inhibitory regulatory module within RyR1 such that channel activity increases when this module is disrupted by either toxin or II-III loop peptide binding. Curiously, although IpTxA strongly influences the gating of isolated RyR1 channels, it does not alter RyR1-mediated Ca^{2+} release during skeletal EC coupling.[7] This suggests that the RyR1 channel becomes insensitive to IpTxA in muscle cells when it is under the control of the DHPR.[7] If the inhibitory regulatory module including the SPRY2 domain is interrupted by binding of IpTxA, then its interruption may similarly have a minimal influence on RyR1-mediated Ca^{2+} release during skeletal EC coupling. However, the impact of the SPRY2 domain regulatory module on RyR1-mediated Ca^{2+} release during EC coupling has not been determined and is examined here.

The impact of a regulatory module containing the SPRY2 domain on Ca^{2+} release during EC coupling was also of interest because SPRY2 is included in a larger N-terminal region of RyR1 that influences conformational DHPR-RyR1 coupling.[4] One loop of the SPRY2 domain (P^{1107}-A^{1121}, the **F** loop) binds to the positively charged α-helical region of the N-terminal part of the DHPR II-III loop (between residues E^{666}-L^{690}).[3,13,14] These basic II-III loop residues do not overlap with the "critical" amino acids (720–765) in the central region of the II-III loop[15] that are required for the conformational coupling between the DHPR and RyR1 that defines skeletal muscle EC coupling. This suggests that SPRY2 domain binding to the II-III loop does not contribute to the essential role of the II-III loop in EC coupling. However, it is possible that the SPRY2 domain influences EC coupling through interaction with another site, but this possibility has not been specifically examined. Here we directly assessed the specific role of the **F** loop of the SPRY2 domain on RyR1 function and investigated the possible role of three specific residues in the **F** loop in regulating in vitro RyR1 channel activity and bi-directional DHPR-RyR1 signaling[16] during EC coupling in myotubes.

We also addressed the likely binding partner for the SPRY2 domain in the inhibitory regulatory module within RyR1. RyR1 contains a region that exhibits close structural and functional similarity to the N-terminal residues of the DHPR II-III loop[17-19] and structural similarity to IpTxA and maurocalcine. This 30 amino acid region in RyR1 contains alternatively spliced (ASI) residues plus a neighboring polybasic sequence and is designated here as the ASI/basic region (T^{3471}-G^{3500}). Although its binding partners are unknown, several lines of evidence indicate that the small ASI/basic region is a functionally very important region in RyR1. Firstly, the variably spliced residues D^{3483}-G^{3487} are present in the adult RyR1 isoform (ASI(+)RyR1), but excluded from the juvenile isoform (ASI(-)RyR1). Secondly, ASI(-)RyR1 is upregulated in adults with myotonic dystrophy.[20] Thirdly, the ASI residues contribute to a regulatory module in the RyR1 complex.[21] Finally, mutations of the ASI residues or adjacent basic residues produce significant effects on skeletal muscle EC coupling.[22,23] Specifically, omission of the 5 variably spliced residues leads to a significant increase in the gain of EC coupling[22] and the cluster of adjacent basic residues (L^{3495}-R^{3499}) contributes to a binding site for the DHPR β_{1a} subunit and its deletion leads to a substantial reduction in voltage-dependent Ca^{2+} release during skeletal EC coupling.[23]

The cluster of positively charged residues in the ASI/basic region and in the N-terminal region of the DHPR II-III loop are aligned along one surface of an α-helix. As a result, there is competition between the positively charged residues in the II-III loop and positively charged residues in the ASI/basic region for in vitro binding to a negatively charged region of RyR1.[22] Therefore, since the negatively charged **F** loop of the SPRY2 domain binds to the DHPR II-III loop in vitro,[14] we predicted that by homology it may also bind to the ASI/basic region. Moreover, there is also evidence that the SPRY2 domain and the ASI/basic region are located within 4–6 nm of each other in the three dimensional RyR1 structure, and thus, could interact (Professor M. Samso, personal communication). The SPRY2 domain has been localized to the clamp region of RyR1 using 3 different anti-SPRY2 antibodies (Perálvarez-Marín A, Tae HS, Board PG, Casarotto MG, Dulhunty AF and Samsó M—in preparation for publication), including the antibody used in the present work (Results, **Figs. 2 and 3**). The ASI/basic region has not been localized on the RyR 3D structure. However the residues are within the IPTxA binding sequence (3,210–3,661) and the IPTxA binding site is located 4 nm from the SPRY2 domain.[5,24] Furthermore, in the linear RyR1 sequence, ASI/basic residues are separated by only 100–150 residues from the calmodulin binding site which is located 6 nm from the SPRY2 domain.[25] Thus, depending on the degree of folding, it is possible that the SPRY2 domain and the ASI/basic regions are close enough to interact to form the inhibitory module that is disrupted by IpTxA, the N-terminal residues of the II-III loop or a peptide corresponding to the RyR1 ASI/basic region.[22] Here, we set out to validate this proposed electrostatic binding interaction between the negatively charged residues in the SPRY2 **F** loop and the positively charged ASI residues and to investigate the possible functional impact of this interaction on RyR1 channel activity in planar lipid bilayers and during physiological ligand and depolarization-induced activation following expression in RyR1-null myotubes.

Results

The role of the SPRY2 domain and its **F** loop in influencing RyR1 channel activity was explored using a peptide with the **F** loop sequence (**F** peptide, Methods) and an antibody to the SPRY2 domain.

A peptide with the SPRY2 F loop sequence activates RyR1 channels. One **F** peptide concentration was tested in each

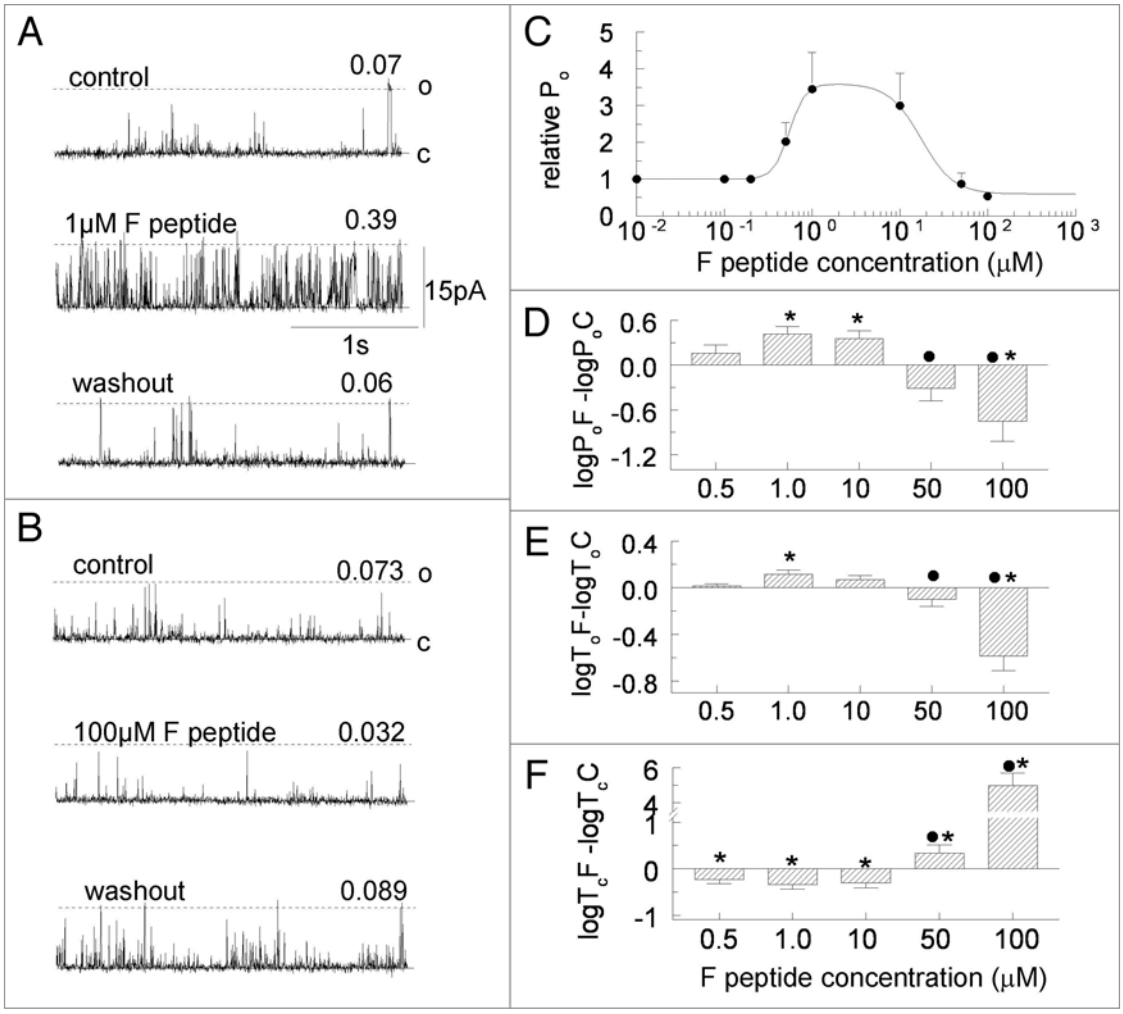

Figure 1. Effects of **F** loop peptide added to the cytoplasmic side of RyR1 channels in lipid bilayers. The representative 3-s traces in (A and B) were recorded at +40 mV, with 10 μM cis (cytoplasmic) Ca^{2+} and 1 mM trans (luminal) Ca^{2+}. Channels open upward from the closed level (c) to the maximum current (o). Each part shows activity, from top down: prior to adding peptide, after 3–5 min with peptide and 3–5 min after peptide washout. (A) 1 μM **F** peptide increased activity. (B) 100 μM **F** peptide reduced activity. Open probability is shown at top right of each trace. (C) average relative open probability (P_o) vs. [**F** peptide]. The line is a least squares fit of the sum of two Hill equations using parameters given in the text. The sum of squares of the difference between the data and the curve was 0.02 μM. (D–F) changes in open probability (P_o), mean open (T_o) and mean closed (T_c) times. (D) relative P_o plotted as ($logP_oF - logP_oC$) for comparison with channel open ($logT_oF - logT_oC$) in (E) and closed ($logT_cF - logT_cC$) times in (F). (*) indicate a significant difference from control and (●) a significant difference between high and low concentration effects.

experiment to evaluate any time-dependent effects on channel activity. The peptide was applied to the cytoplasmic solution and channel activity followed for ~20 min before the peptide was removed by perfusion. The peptide at 1 to 10 μM (**Fig. 1A**) activated channels, while higher concentrations (100 μM) inhibited. No time-dependent effects were seen; channel activity changed within 30 s of peptide application and was maintained until the peptide was removed. Bilayers were maintained through to washout in at least one or two experiments at each peptide concentration. In each case, activity returned to control levels within 1–2 min as shown in **Figure 1A and B**.

The average values in **Figures 1, 3 and 4** combine data at +40 and -40 mV for simplicity of presentation as there was no consistent difference between parameters obtained at the two potentials (**Table 1A**). Data for each channel was normalized to its internal control to avoid anomalies introduced by the usual variability in baseline gating between RyR1 channels,[26,27] which is reflected in the range of control values in **Table 1B**. The results in **Figure 1A–C** are consistent with a higher affinity activation by 1–10 μM **F** peptide and a lower affinity inhibition with ≥50 μM peptide. The fit to the data in **Figure 1C** with standard Hill equations (Methods) show an AC_{50} of 0.55 μM and Hill coefficient of 4.8 for activation, and an IC_{50} of 17.4 μM and Hill coefficient of 2.4 for inhibition. The coefficient of ~4 for activation suggests that the **F** peptide binds to four high affinity sites on the RyR1 complex, perhaps to one binding site per subunit. The coefficient of 2.4 for inhibition suggests that low affinity binding to only two subunits may be required for inhibition.

The effects of the **F** peptide on channel gating are shown as the average difference between log_{10} of each control and test

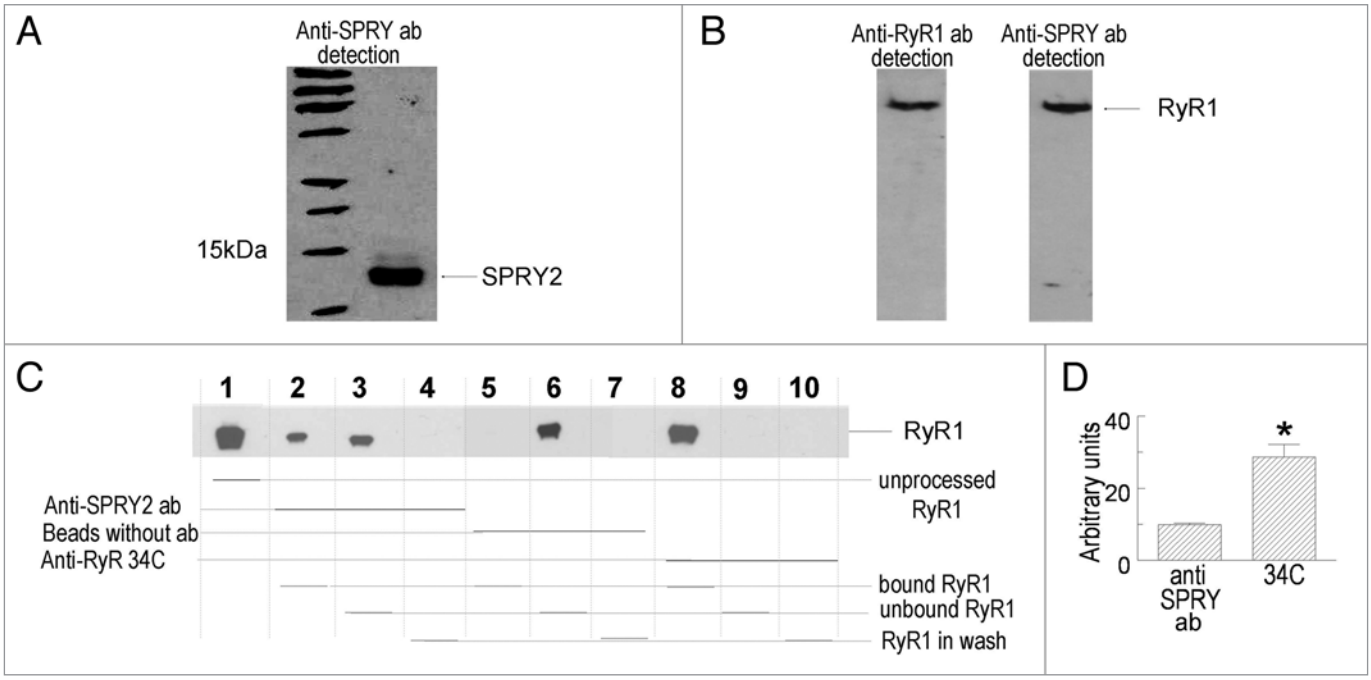

Figure 2. Characterization of the SPRY2 antibody. (A) the SPRY2 antibody detected the recombinant SPRY2 domain (in three of three trials). (B) RyR1 in SR vesicles was detected using either the 34C antibody (0.05 ug/ml) (Abcam Cambridge, MA USA) (left) or SPRY2 antibody (2 ug/ml) (right) following transfer from native gels (in six of six trials with vesicles from two different preparations). (C) comparison of the ability of the anti-SPRY2 antibody and the commercially available 34C antibody to immunoprecipitate purified RyR1 protein. Lane 1 contains 32 ng purified RyR1 (positive control, not exposed to beads). Lanes 2, 3 and 4-Protein A-Sepharose beads incubated with anti-SPRY2 antibody (2 ug/ml). Lanes 5, 6 and 7-Protein A-Sepharose beads lacking bound antibody (negative control). Lanes 8, 9 and 10-Protein A-Sepharose beads with 34C. Lanes 2, 5 and 8 contain RyR1 bound to beads (i.e., in the pellet) after centrifugation. Lanes 3, 6 and 9 contain unbound RyR1 (i.e., in the supernatant) after centrifugation. Lanes 4, 7 and 10 show RyR1 in the supernatant after washing the beads. In each experiment, the beads (with or without antibody) were exposed to RyR1 diluted to 25 μg/ml. (D) shows the average results of densitometry scans of RyR1 immunoprecipitated by the Anti-SPRY2 antibody and RyR1 immunoprecipitated by the 34C antibody (n = 3 for each average).

parameter (**Fig. 1D–F**). The increase in channel open probability with 1 and 10 μM **F** peptide and the decline in activity at 50 and 100 μM **F** peptide are significant and are accompanied by small changes in mean open time and larger changes in mean closed times. The open times with 1 μM peptide were significantly longer and closed durations were significantly shorter than control with 0.5, 1 and 10 μM peptide. Open times with the **F** peptide at 50 and 100 μM were significantly shorter than with 0.5, 1 and 10 μM, while closed times were significantly longer. When compared to control, the open times with 100 μM peptide were significantly shorter, and mean closed time significantly longer. Control experiments with unrelated peptides were not conducted here as we previously demonstrated the absence of effects on RyR1 activity of several unrelated peptides.[22,28,29] Moreover, the lack of stimulation of the SPRY2 RyR1 mutant by the **F** loop peptide in **Figure 4** provides an additional important negative control for **F** loop peptide specificity.

One interpretation of the increase in RyR1 activity with low **F** loop peptide concentrations is that the peptide disrupts a closed state stabilization module in RyR1 involving an interaction between the endogenous SPRY2 **F** loop and another part of the RyR1 protein complex. As suggested for the actions of other domain peptides,[30] the **F** loop peptide could bind and displace the endogenous **F** loop binding partner. Support for this proposed mechanism can be inferred from experiments in which an antibody to the domain peptide exerts a similar action, presumably by binding to the endogenous domain to interrupt the same inhibitory module.[31] Thus we examined the actions of a polyclonal antibody raised against the SPRY2 domain. Since the homology model of SPRY2 shows that the **F** loop is on the outer surface of the domain,[3,14] it was likely that the **F** loop region provided an epitope for antibody recognition in the polyclonal mixture.

The antibody to the SPRY-2 domain alters RyR1 channel activity. Western blots show that the anti-SPRY2 antibody recognized the recombinant SPRY2 domain (**Fig. 2A**) and native RyR1 channels in SR vesicles (**Fig. 2B**). Moreover, the antibody immunoprecipitated purified RyR1, but with a lower efficacy than the widely used anti-RyR 34C antibody (**Fig. 2C and D**, for details see Methods).

Addition of the anti-SPRY2 antibody to the cytoplasmic solution caused changes in open probability similar to those with the **F** loop peptide (**Fig. 3A**). Specifically, 1 μg/ml anti-SPRY2 antibody substantially increased RyR1 activity, while 5 μg/ml nearly abolished activity. Both the increase and the decrease in activity were seen within 30 s of antibody addition and maintained for 10–30 min. The antibody concentration was increased further to 10 μg/ml in three experiments, and to 20 μg/ml then 40 μg/ml in another, but no further decrease in activity was detected below

that recorded with 5 μg/ml of the antibody. The purified anti-γ-GCT antibody had no effect on channel activity in six experiments (**Fig. 3B**).

On average, 1 μg/ml of the anti-SPRY2 antibody caused a significant increase in open probability and 5 μg/ml produced a significant decrease to values less than that of control (**Fig. 3C**). In marked contrast, relative channel open probability (P_o) was unaltered by the control anti-γ-GCT antibody (1 or 5 μg/ml, or even 10 μg/ml in one experiment). The average basal P_o was 0.14 ± 0.04 for the anti-SPRY2 antibody experiments and 0.19 ± 0.08 for anti-γ-GCT experiments. The changes in open probability with the anti-SPRY2 antibody were due to opposing effects on channel open (**Fig. 3D**) and closed (**Fig. 3E**) times. With 1 μg/ml anti-SPRY2 antibody, the relative open time increased significantly (from 3.2 ± 0.6 ms), while the relative closed time fell significantly (from 82.0 ± 31.5 ms). When anti-SPRY2 antibody was increased to 5 μg/ml, the relative open time fell significantly below control while the relative closed time increased significantly. The basal open and closed times before antibody addition were 3.2 ± 0.6 ms and 82.0 ± 31.5 ms, respectively. Neither 1 μg/ml nor 5 μg/ml anti-γ-GCT antibody altered either open (control, 4.35 ± 1.35 ms) or closed times (control, 73.5 ± 33.2 ms). Thus, the anti-SPRY2 antibody regulates RyR1 channels in a qualitatively similar biphasic manner as that of the SPRY2 **F** loop peptide.

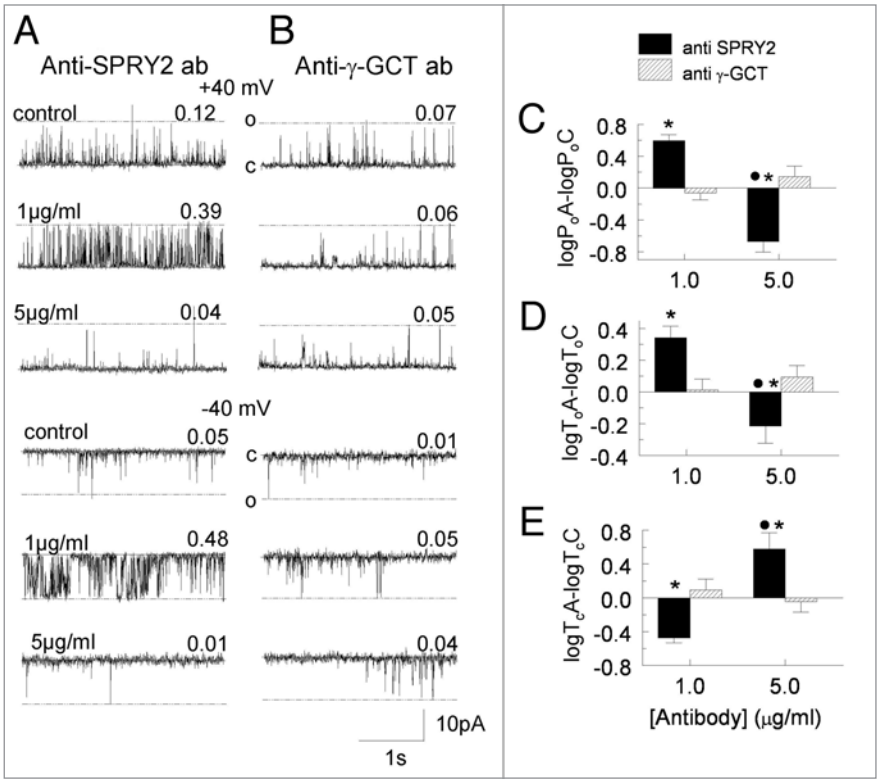

Figure 3. (A and B) effects of anti-SPRY2 and anti-γ-GCT antibodies on the cytoplasmic side of RyR1 channels in lipid bilayers. The 3s recordings were at +40 mV (upper) or -40 mV (lower) with 10 μM cis and 1 mM trans Ca^{2+}. Channels open upward at +40 mV or downward at -40 mV from zero (c) to the maximum channel current (o). Each part shows 3 s of activity, from the top down: prior to antibody (control), after 3–5 min with 1 μg/ml antibody and 3–5 min after increasing the antibody to 5 μg/ml. Open probability is given at the top right of each trace. (C–E) average changes in open probability, open and closed times with the antibodies (P_oA, T_oA and T_oC), plotted in the same way as in Figure 1. (*) indicates a significant difference from control and (●) a significant difference between responses to the anti-SPRY2 and anti-γ-GCT antibodies.

Overall, the results in **Figures 1–3** suggest that the **F** loop of the SPRY2 domain is a functionally significant modulator of RyR1 channel gating. We next examined the **F** loop contribution to a protein-protein interaction(s) within the RyR1 complex, and whether this interaction significantly impacts channel activity and EC coupling. The activating effect of the **F** loop and SPRY2 antibody on RyR1 is similar to previously reported effects of the ASI/basic peptide.[21] The ASI/basic region contains a stretch of positively charged residues that could interact with acidic residues in the SPRY2 F loop to form a regulatory module within RyR1. The involvement of the SPRY2 **F** loop in an inter-domain interaction with the ASI region was first explored in biochemical experiments to examine the ability of the two regions to bind to each other.

The basic residues in the ASI/basic region influence its binding to the SPRY2 domain. The binding of the recombinant SPRY2 domain to two peptides corresponding to the ASI/basic region was examined. These peptides (see Methods) were; (1) ASI(+) containing the variably spliced residues, (2) ASI(-) lacking the residues and (3) two ASI(-) mutants. The ASI(-) peptide bound to the SPRY2 domain with a K_d of 1.5 ± 0.1 μM (**Table 2**), which was >4-fold lower than K_d for the ASI(+) peptide (6.6 ± 0.2 μM). The higher affinity for the ASI(-) peptide is reminiscent of its 4- to 6-fold higher affinity for RyR1 in [^{3}H]ryanodine binding experiments and its greater ability to increase SR Ca^{2+} release and enhance RyR1 channel activity, with affinities also in the 1–10 μM range.[21]

The influence of the ASI peptides on RyR1 activity depends on the peptides having an α-helical structure with positively charged residues aligned on one side of the helix.[22] Therefore, we determined the impact of this positive charge density and α-helical structure on ASI peptide binding to the SPRY2 domain using two mutant ASI(-) peptides. In the 1st mutant ($ASI(-)_{mutant}$), three positively charged residues were substituted with alanine or leucine (K3495A, K3496A and R3498L). This peptide retains an α-helical structure, but has limited ability to activate RyR1.[22] Its affinity for binding to the SPRY2 domain was reduced >8-fold (**Table 2A**). The second mutant, ASI_{short} (R^{3493}-G^{3500}), retains the positively charged residues, but is too short to sustain an α-helical structure. ASI_{short} was relatively ineffective in activating RyR1,[22] and its affinity for the SPRY2 domain was reduced >10-fold (**Table 2A**). Thus, the charge and structure of the ASI/basic

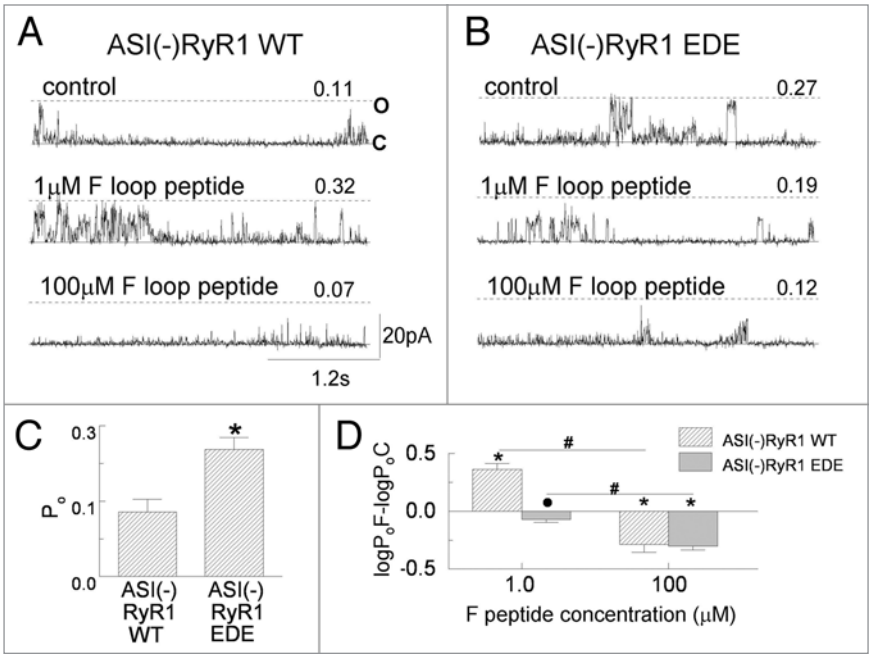

Figure 4. Actions of the **F** loop peptide on recombinant ASI(-)RyR1 WT and the SPRY-2 domain mutant ASI(-)RyR1 EDE incorporated into lipid bilayers. (A and B) show effects of **F** loop peptide applied to the cytoplasmic side of RyR1 channels in lipid bilayers. The 3 s recordings were at +40 mV with 10 μM cis and 1 mM trans Ca^{2+}. Channels open from the zero current level (c) to the maximum channel current (o). Each part shows 3 s of activity, from the top down: prior to **F** loop peptide addition (control), after 3–5 min with 1 μM peptide and 3–5 min after increasing the peptide concentration to 100 μM. Open probability is given at the top right of each trace. (C) average open probability under control conditions before addition of the **F** loop peptide for ASI(-)RyR1 WT and ASI(-)RyR1 EDE. (D) average changes in open probability with the **F** loop peptide plotted in the same way as data in Figure 1. (*) indicates a significant difference from control and (●) a significant difference between responses to the anti-SPRY2 and anti-γ-GCT antibodies.

Table 1A. Effects of **F** loop peptides on native RyR1 in SR isolated from rabbit skeletal muscle are independent of bilayer potential

(A). Peptide	Bilayer voltage	Relative P_o	Relative T_o	Relative T_c
10 (μM)	-40 mV	3.4 ± 1.7	1.15 ± 0.08	0.66 ± 0.16
	+40 mV	2.6 ± 0.68	1.28 ± 0.22	0.58 ± 0.15
50 (μM)	-40 mV	0.93 ± 0.41	0.92 ± 0.16	3.02 ± 1.7
	+40 mV	0.79 ± 0.53	0.76 ± 0.23	2.40 ± 1.00

Average P_o, T_o and T_c with 10 μM (activating) and 50 μM (inhibiting) peptide, relative to the internal control for each channel before peptide addition at -40 or +40 mV. Mean ± sem (n = 5–7).

region dictates its interaction with the SPRY2 domain and its regulation of RyR1 activity in a very similar way, consistent with the hypothesis that the ASI region may regulate RyR1 through binding to the SPRY2 domain.

Residues in the SPRY2 domain required for binding to the ASI/basic region. One acidic residue E^{1108} in a negatively charged region of the SPRY2 **F** loop influences its in vitro binding to the basic N-terminal region of the DHPR II-III loop.[22] Thus, we tested if the same acidic region also interacts with basic residues in the α-helix of the structurally analogous ASI/basic region. The E1108A **F** loop substitution reduced the affinity for ASI(-) ~7-fold (mutant-1, **Table 2B**). The D1112A substitution (Mutant-2) caused a 9-fold decline in affinity. Mutating both residues (mutant-6) produced a 19-fold fall in affinity, while an additional E1114A (mutant-7) substitution abolished binding. Curiously, however, neither the single E1114A substitution (mutant-3), D1118A (mutant-4) nor E1119A (mutant-5) alone significantly altered binding. Thus, E^{1108}, D^{1112} and E^{1114} are essential for in vitro binding of the SPRY2 domain to the ASI/basic residues. Mutation of the three acidic residues abolished SRRY2 domain binding to the ASI/basic region, in contrast to only a partial reduction in SPRY2 binding to the N-terminal residues of the II-III loop with E1108A.[14] This observation indicates that the binding site for the N-terminal residues of the II-III loop and for the ASI/basic region overlap but is not identical. However, the overlap may be sufficient for binding of the N-terminal II-III loop residues to disrupt the interaction between the **F**-loop and the ASI/basic region.

Impact of SPRY2 binding to ASI(-)/basic residues on in vitro RyR1 function. The results thus far demonstrate that the isolated ASI/basic region binds to the SPRY2 domain in RyR1. We reported that the ASI/basic residues of RyR1 strongly impact RyR1 activity and EC coupling.[22] Specifically, the ASI(-) peptide activates RyR to a greater extent than the ASI(+) peptide and full-length juvenile ASI(-) RyR1 exhibits enhanced depolarization-induced Ca^{2+} release compared to the adult ASI(+)RyR1.[22] This gain in function in the full-length ASI(-)RyR1 may reflect a tighter interaction between the SPRY2 domain and ASI(-)/basic region. Thus, we tested the hypothesis that the strength of EC coupling depends on SPRY2/basic interaction by assessing the effects on RyR1 channel activity and EC coupling of mutations in the SPRY2 domain that disrupt binding of the domain to the ASI(-) peptide. For these experiments, the SPRY2 domain residues E^{1108}, D^{1112} and E^{1114} were substituted with alanines in the full-length juvenile ASI(-) RyR1 since these three mutations abolished in vitro binding of the SPRY2 domain to the ASI region (mutant-7, **Table 2B**). We predicted that the SPRY2 domain mutations would disrupt the SPRY2-ASI/basic inhibitory interaction, increase isolated RyR1 channel activity and enhance Ca^{2+} release during EC coupling.

We first determined the effect of the three mutations on regulation of ASI(-)RyR1 single channel activity by the **F** loop peptide (**Fig. 4**). Wild-type ASI(-)(ASI(-)RyR1 WT) and the ASI(-)RyR1 triple mutant (E^{1108}A, D^{1112}A and E^{1114}A, ASI(-) RyR1 EDE) were expressed in HEK293 cells and the RyR1 protein was solubilized and incorporated into lipid bilayers (**Fig. 4A and B**). As predicted, the average basal channel open probability

Table 1B. Average control P_o, T_o and T_c before adding peptide, included to indicate baseline values for each parameter and the variability of control channel gating which necessitates normalization of test parameters

(B). Control parameters for the following experiments		P_o	T_o (ms)	T_c (ms)
F loop peptide: 0.5 μM	Mean ± sem (14)	0.013 ± 0.003	1.54 ± 0.95	195 ± 31
	range	0.002–0.037	1.08–2.26	57–588
1.0 μM	Mean ± sem (10)	0.035 ± 0.014	1.47 ± 0.14	762 ± 370
	range	0.0003–0.13	0.95–2.14	14–3472
10 μM	Mean ± sem (10)	0.050 ± 0.020	1.78 ± 0.29	167 ± 68
	range	0.003–0.11	1.0–3.6	12–631
50 μM	Mean ± sem (10)	0.032 ± 0.015	1.96 ± 0.26	189 ± 51
	range	0.005–0.12	1.4–3.6	16–430
100 μM	Mean ± sem (5)	0.108 ± 0.044	3.16 ± 0.60	86 ± 50
	range	0.005–0.27	1.83–4.26	8–224

Table 2. K_d for wild-type and mutant ASI/basic peptide binding to recombinant wild-type SPRY2 domain (A) and wild-type ASI(-)/basic peptide binding to wild-type and mutant SPRY2 domain constructs (B)

(A). ASI/basic peptides	Dissociation constant, K_d (μM)	(B). SPRY2 constructs	Dissociation constant, K_d (μM)
1. Peptide ASI(-)	1.5 ± 0.1	Wild-type P^{1107}ELRPDVELGADELA^{1121}	1.5 ± 0.1
2. Peptide ASI(+)	6.6 ± 0.2	Mutant-1 P^{1107}**A**LRPDVELGADELA^{1121}	9.7 ± 0.1
3. Peptide ASI(-)$_{mutant}$	12.4 ± 0.6	Mutant-2 P^{1107}ELRP**A**VELGADELA^{1121}	13.2 ± 0.4
4. Peptide ASI$_{short}$	15.1 ± 0.2	Mutant-3 P^{1107}ELRPDV**A**LGADELA^{1121}	1.7 ± 0.1
		Mutant-4 P^{1107}ELRPDVELGA**A**ELA^{1121}	1.5 ± 0.1
		Mutant-5 P^{1107}ELRPDVELGAD**A**LA^{1121}	1.58 ± 0.1
		Mutant-6 P^{1107}**A**LRP**A**VELGADELA^{1121}	27.04 ± 0.2
		Mutant-7 P^{1107}**A**LRP**A**V**A**LGADELA^{1121}	NB
		Mutant-8 P^{1107}**A**LRP**A**V**A**LGA**A**LA^{1121}	NB

K_d obtained from non-linear regression fits to quenching of intrinsic SPRY2 domain tryptophan fluorescence by ASI/basic peptides (n = 3) (Methods, $R^2 > 0.96$). NB indicates no binding.

of the ASI(-)RyR1 EDE was significantly greater than that of ASI(-)RyR1 WT (**Fig. 4C**). The **F** loop peptide was added to cytoplasmic solution bathing the channels firstly at a concentration of 1 μM, and then the concentration was increased after 5–8 min to 100 μM. Similar to ASI(+) RyR1 (**Fig. 1**), ASI(-) RyR1 WT channels responded to 1 μM **F** loop peptide with an increase in activity (P_o increased from 0.13 ± 0.03 to 0.34 ± 0.07) and then activity decreased below control levels after increasing the peptide concentration to 100 μM (to 0.083 ± 0.02, **Fig. 4A and D**). In marked contrast, the open probability of ASI(-) RyR1 EDE channels did not change significantly with 1 μM **F** loop peptide (P_o: control 0.25 ± 0.02; F-loop, 0.25 ± 0.03) and decreased substantially after addition of 100 μM of the peptide (P_o reduced to 0.16 ± 0.02; **Fig. 4B and D**). Thus, the SPRY2 mutations selectively abolished channel activation by low concentrations of **F** loop peptide.

SPRY2 binding to ASI(-)/basic residues does not alter cellular RyR1 function or bi-directional DHPR-RYR1 signaling during EC coupling. We next examined the possible impact of the SPRY2 mutations in ASI(-)RyR1 on RyR1 function and bi-directional DHPR-RyR1 signaling during EC coupling following expression in RyR1-null myotubes and HEK-293 cells (**Figs. 5 and 6**). **Figure 5A** shows representative electrically evoked and ligand-induced (30 mM caffeine and 500 μM 4-CMC) responses from indo-1 am-loaded RyR1-null myotubes expressing either wild-type ASI(-) (ASI(-)RyR1 WT) or the ASI(-)RyR1 triple mutant (ASI(-)RyR1 EDE). Average peak responses to each stimulus are summarized in **Figure 5B** and were not significantly different between RyR1-null myotubes expressing either ASI(-) RyR1 WT or ASI(-)RyR1 EDE. As shown previously in reference 32, peak electrically-evoked Ca^{2+} transient amplitude is smaller than that produced by exposure to caffeine and 4-CMC due to the much longer RyR1 activation during ligand activation (30 s) compared to that produced by a single action potential stimulus (~10 ms). In addition, following expression in HEK293 cells, the magnitude and sensitivity of 4-CMC-induced Ca^{2+} release was also similar for ASI(-)RyR1 WT (**Fig. 5C** filled circle; ΔR_{max} = 1.3, EC_{50} = 97 μM and Hill coefficient = 1.4) and ASI(-)RyR1 EDE (**Fig. 5C** open circle; ΔR_{max} = 1.4, EC_{50} = 113 μM and Hill coefficient = 1.3).

The effects of the SPRY2 domain mutations that disrupt binding to the ASI(-) region on bi-directional DHPR-RyR1 coupling are summarized in **Figure 6**. The whole-cell voltage clamp technique was used to simultaneously record

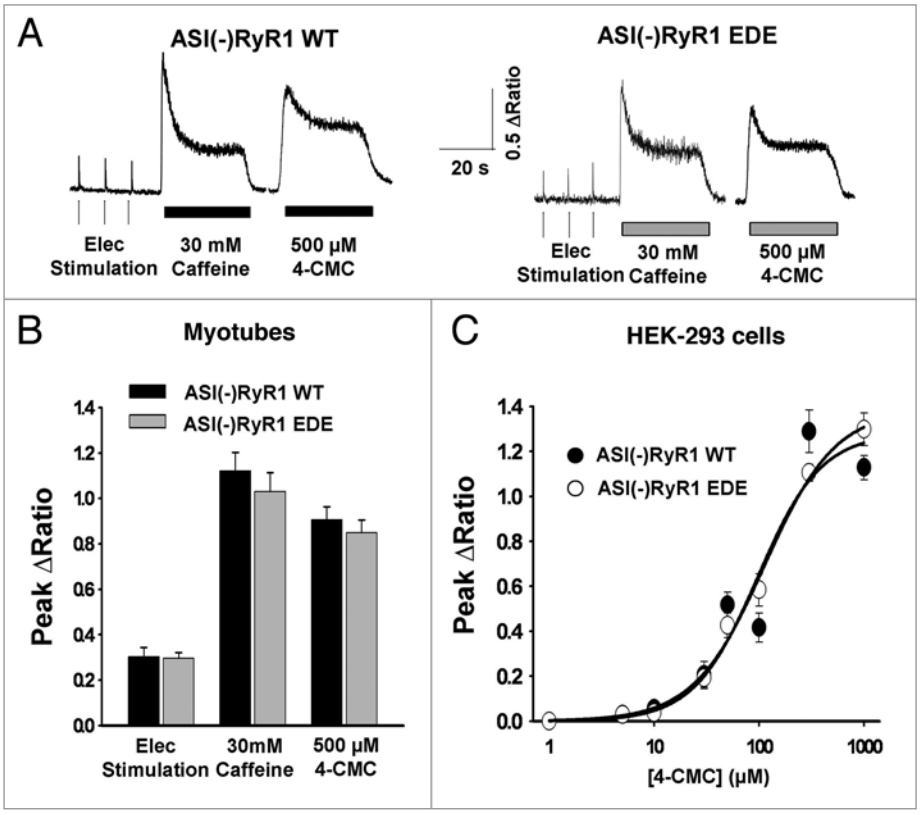

Figure 5. (A and B) Electrically-evoked and ligand-induced Ca^{2+} release in indo-1-loaded RyR1-null myotubes expressing either ASI(-)RyR1 WT or the ASI(-)RyR1 $E^{1108}A/D^{1112}A/E^{1114}A$ triple mutant (ASI(-)RyR1 EDE). (A) representative responses from ASI(-)RyR1 WT-expressing (left) and ASI(-)RyR1 EDE-expressing (right) myotubes to electrical stimulation (vertical lines) and sequential 30s applications of 30 mM caffeine and 500 μM 4-CMC. (B) average peak amplitude of electrically-evoked, caffeine-induced and 4-CMC-induced Ca^{2+} transients in ASI(-)RyR1 WT- (solid bars) and ASI(-)RyR1 EDE- (light grey bars) expressing myotubes. (C) 4-CMC-induced Ca^{2+} release concentration-response curves (fitted with Hill equation) obtained from HEK293 cells expressing either ASI(-)RyR1 WT (filled circles) or ASI(-)RyR1 EDE (open circles).

depolarization-induced L-type Ca^{2+} currents and intracellular Ca^{2+} transients in RyR-null myotubes expressing either ASI(-)RyR1 WT, the $E^{1108}A$, $D^{1112}A$ ASI(-) double mutant (ASI(-)RyR1 ED) or ASI(-)RyR1 EDE. The voltage dependence and peak magnitude of both L-type Ca^{2+} currents (**Fig. 6A and C and Table 3**) and intracellular Ca^{2+} transients (**Fig. 6B and D and Table 3**) were similar for all three constructs. A small (~6 mV) depolarizing shift in the voltage dependence L-type Ca^{2+} channel activation was the only parameter significantly altered by both the ED and EDE SPRY2 domain mutations (**Fig. 6C and Table 3**). The SPRY2 domain ED double mutant introduced into full-length adult ASI(+)RyR1 also did not significantly alter the magnitude or voltage dependence of either L-type Ca^{2+} currents or intracellular Ca^{2+} transients (data not shown). Together, the results in **Figures 5 and 6** demonstrate that the bi-directional DHPR-RyR1 signaling is not dramatically altered by **F** loop mutations that destabilize an interaction between the SPRY2 and ASI domains in vitro. It is possible that the influence of the SPRY2-ASI/basic interaction on RyR1 activity observed in vitro is masked by interactions of the channel with other proteins present within cells.

Discussion

The data presented in this study provides several novel observations and raises a number of new questions. Our results are the first to demonstrate that the SPRY2 domain binds to the ASI/basic region in RyR1 (**Table 2**) and regulates RyR1 channel activity (**Fig. 1**), but that this interaction is not an essential determinant of in situ RyR1 function or bi-directional DHPR-RyR1 coupling in myotubes (**Figs. 5 and 6; Table 3**). The SPRY2-ASI/basic regulatory interaction is indicated by similar stimulatory effects on RyR1 activity by low concentrations of both a peptide corresponding to the SPRY2 domain **F** loop and an antibody to the SPRY2 domain. Moreover, we demonstrated direct binding between the SPRY2 **F** loop and ASI/basic peptides and that this interaction is strongly influenced by three specific acidic residues in the SPRY2 **F** loop. Disruption of the putative ASI/SPRY2 interaction by mutating these acidic residues in the full-length protein increased the RyR1 channel open probability, abolished channel activation by low concentrations of **F** loop peptide, but did not significantly alter either ligand- or depolarization-induced RyR1 Ca^{2+} release following expression in RyR1-null myotubes and HEK293 cells. These results indicate that while SPRY2 contributes to an in vitro RyR1 regulatory domain, the influence of this domain is substantially reduced in intact cells, under the conditions examined here. Thus, although the SPRY2 domain (aa 1,085–1,208) is contained within regions of RyR1 shown to influence skeletal muscle EC coupling (aa 1–1,681),[4] our results suggest that these effects do not involve a regulatory module including the three acidic **F** loop residues required for intramolecular binding to the ASI/basic region.

F loop peptide and anti SPRY2 domain antibody modulation of RyR1. Both the **F** peptide (**Fig. 1**) and the anti SPRY2 antibody (**Fig. 3**) activate RyR1 channels at low concentrations, the **F** peptide with a Hill coefficient of ~4. This suggests that the SPRY2 domain may contribute to an intramolecular inhibitory module in each subunit of the RyR1 tetramer and that competing **F** loop peptide and anti-SPRY2 antibody activates the channel by disrupting the four inhibitory modules within the RyR1 tetramer.

The dual effects of the peptide and antibody on RyR1 channel activity (activation at low and inhibition at high concentrations) could potentially be due to the peptide and the antibody binding to two sites on RyR1 with the lower affinity interaction being non-specific. Alternatively, the biphasic effect could arise from

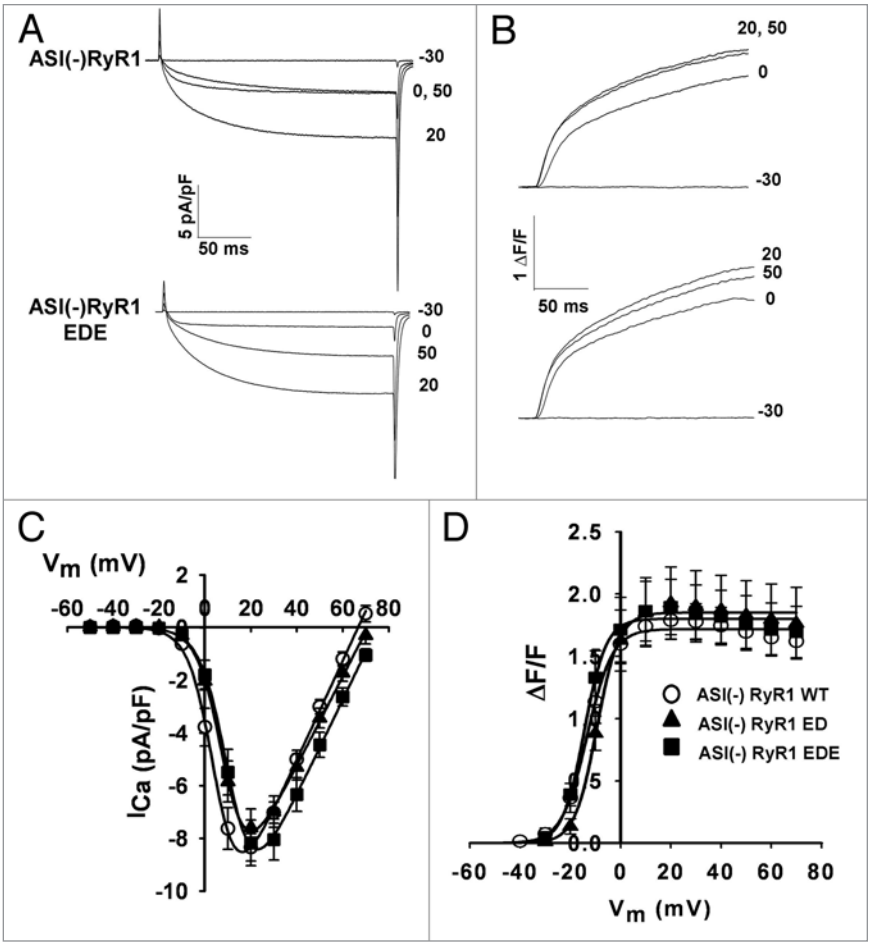

Figure 6. Effect of SPRY domain mutants on bi-directional DHPR-RyR1signaling and EC coupling in RyR1-null myotubes. (A and B), representative L-type Ca^{2+} currents (A) and Ca^{2+} transients (B) elicited by 200 ms depolarizations to -30, 0, 20 and 50 mV in ASI(-)RyR1 WT- (upper) and ASI(-)RyR1 EDE-expressing (lower) myotubes. (C and D), average voltage dependence of peak L-type Ca^{2+} current density (C) and intracellular Ca^{2+} transients (D) from ASI(-)RyR WT- (○), ASI(-)RyR1 ED- (▲), and ASI(-)RyR1 EDE-expressing (■) myotubes.

the binding of peptide or antibody to a common site in which activation and inhibition reflect binding to a different number of RyR1 subunits. However, our finding that channel activation by low concentrations of **F** loop peptide was selectively abolished by mutations in the SPRY2 domain that disrupt its interaction with the ASI region, but not the inhibition observed at high concentrations of **F** peptide suggests that the biphasic effect most likely reflects binding to two distinct sites.

Parallel effects of antibodies and peptides on release channel function have previously been interpreted in terms of interruption of important intramolecular regulatory domains that involve interactions between different regions of RyR1.[30,31] Within this framework, our results are consistent with the SPRY2 **F** loop being involved in a functionally important inhibitory module of the channel. Although we found that the **F** loop peptide binds with relatively high affinity to the ASI/basic region, the myotube RyR1 reconstitution studies suggest that the ASI/basic region may not serve as the physiologically relevant binding site in intact muscle cells.

The SPRY2-ASI/basic interaction. We defined essential structural parameters required for the ASI/basic region to interact with the SPRY2 domain. The interaction site on the ASI peptide involves a series of basic residues aligned along one side of an α-helix. Both neutralization of the basic residues and disruption of the α-helix reduce the affinity of the ASI/basic region for the SPRY2 domain, although the remaining lower affinity binding is consistent with other residues in the ASI/basic region contributing to binding (**Table 2**). Conversely, the substitution of three acidic residues, E^{1108}, D^{1112} and E^{1114} on the SPRY2 **F** loop with non-charged alanine residues abolished binding, indicating a tightly circumscribed binding site on the **F** loop (**Table 2**). In addition, the SPRY2 domain binds to the ASI/basic region with higher affinity than to the N-terminal II-III loop residues, indicating a tighter and more constrained binding interaction between ASI/basic residues and the SPRY2 domain.

A surprising finding was that mutations that abolish SPRY2 domain binding to the ASI/basic region did not significantly impact either ligand-induced RyR1 Ca^{2+} release or bi-directional DHPR-RyR1 signaling (**Figs. 5 and 6 and Table 3**). Thus, although the ASI/basic region strongly influences depolarization-induced Ca^{2+} release during skeletal muscle EC coupling,[22,23] this regulation appears not to depend on an interaction with the SPRY2 domain. Alternatively, the SPRY2-ASI/basic interaction may influence in situ RyR1 function and EC coupling and the absence of a detectable functional effect in myotube experiments could reflect failure of the three mutations to disrupt the interaction in the full-length protein. However, the fact that the mutations selectively abolished the stimulatory effect of the **F** loop peptide on recombinant RyR1 single channel activity suggests that the mutations indeed disrupts the interaction even in the full-length protein. Another possibility is that the effect of ASI/basic region on EC coupling reported previously,[22] reflects modifications of its interaction with the DHPR β_{1a} subunit[23] in a manner that enhances opening of the RyR1 pore to release SR Ca^{2+} during membrane depolarization.

A final possibility is that the influence of the ASI/basic regulatory module on native RyR1 activity is negated by conditions that exist in the cellular environment. For example, the DHPR-RyR1 physical interaction that defines skeletal muscle EC coupling[33] may override or interrupt the SPRY2-ASI regulatory interaction, as it interrupts the IpTxA interaction with RyR1.[7] However the observation that the SPRY2/ASI/basic interaction does not alter 4-CMC induced Ca^{2+} release in HEK293 cells suggests that other factors are involved in interrupting the functional effects

Table 3. Parameters for fitted *I-V* and *F-V* curves

	N	*I-V* data				*F-V* data		
		G_{max} (nS/nF)	k_G (mV)	$V_{G1/2}$ (mV)	V_{rev} (mV)	$(\Delta F/F)_{max}$	k_F (mV)	$V_{F1/2}$ (mV)
ASI(-) WT	12	189 ± 10	4.1 ± 0.2	5.0 ± 1.4	67.0 ± 1.6	1.6 ± 0.2	4.5 ± 0.4	-13.4 ± 1.7
ASI(-) ED	8	176 ± 17	5.4 ± 0.2	10.8 ± 1.6*	73.9 ± 1.6	1.9 ± 0.3	4.2 ± 0.8	-9.2 ± 1.7
ASI(-) EDE	13	176 ± 14	5.3 ± 0.2	11.7 ± 0.9*	74.8 ± 1.1	1.7 ± 0.2	4.8 ± 0.6	-13.4 ± 1.9

Parameters for the voltage dependence of L-type Ca^{2+} channel conductance (I-*V* data) and Ca^{2+} release (*F-V* data) obtained by fitting data from myotubes within each group to the appropriate equations described in Methods. G_{max}, maximal L-channel conductance; $(\Delta F/F)_{max}$, maximal change in relative fluo-4 fluorescence; V_{rev}, L-channel reversal potential; $V_{G1/2}$ and $V_{F1/2}$, potential at which G and F are half-maximal, respectively; k_G and k_F, slope factors for *I-V* and *F-V* curves, respectively. *$p < 0.05$ compared to ASI(-)RyR WT.

of the interaction in cells. These factors might include inhibition by interactions between adjacent RyR1 tetramers assembled in orthogonal arrays, oxidation state or by the regulatory interaction being overwhelmed by the strong positive feedback of Ca^{2+}-induced Ca^{2+} release, where free Ca^{2+} is not held constant as it is in the bilayer studies.

Thus, the in vivo function of the SPRY2 domain and its interaction with the ASI-basic region remains elusive. The fact that it is interrupted by cellular factors present under normal conditions in myotubes and HEK293 cells suggests that any in vivo functional importance may emerge only when the normal cellular conditions are altered as in disease (e.g., myotonic dystrophy) or in aging. The overall effect of interrupting such an inhibitory interaction in muscle during disease or aging would be to allow enhanced activation of the RyR1 during excitation-contraction coupling. These possibilities remain to be explored.

Materials and Methods

Synthetic peptides. The following peptides were synthesized by the JCSMR Biomolecular Resource Facility using an Applied Biosystems 430A Peptide Synthesiser, with purification to 98–100% using HPLC and mass spectroscopy. Stock peptide (5 mM) in H_2O was frozen in 20 μl aliquots.

ASI(+):
T^{3471}ADSKSKMAKAGDAQSGGSDQERTKKKRRG^{3500}

ASI(-):
T^{3471}ADSKSKMAK---------SGG SDQERTKKKRRG^{3500}

ASI(-)$_{mutant}$:
T^{3471}ADSKSKMAK----------SGGSDQERTAAKLRG^{3500}

ASI$_{short}$:
R^{3493}TKKKRRG^{3500}

SPRY2 **F** loop:
CR^{1106}PELRPDVELGADEL^{1120}

Expression of wild-type and mutant SPRY2 domain recombinant proteins. The cDNA encoding the entire SPRY2 domain was amplified by PCR and cloned in-frame down stream of a poly-histidine-tagged ubiquitin sequence in the plasmid pHUE.[13,14] The wild-type and mutant **F** loop sequences in the SPRY2 domain were:

Wild-type	P^{1107}ELR PDV ELG ADE LA^{1121}
Mutant-1	P^{1107}**A**LR PDV ELG ADE LA^{1121}
Mutant-2	P^{1107}ELR P**A**V ELG ADE LA^{1121}
Mutant-3	P^{1107}ELR PDV **A**LG ADE LA^{1121}
Mutant-4	P^{1107}ELR PDV ELG AA**E** LA^{1121}
Mutant-5	P^{1107}ELR PDV ELG AD**A** LA^{1121}
Mutant-6	P^{1107}**A**LR P**A**V ELG ADE LA^{1121}
Mutant-7	P^{1107}**A**LR P**A**V **A**LG ADE LA^{1121}
Mutant-8	P^{1107}**A**LR P**A**V **A**LG **AAA** LA^{1121}

Polyclonal anti-SPRY2 domain antibody. The antibody was produced in rabbits using standard procedures with Freund's adjuvant and three weekly immunizations with purified recombinant SPRY2 domain. The antibody was purified by specific binding to purified SPRY2 domain immobilised on nitrocellulose membranes.[34] The anti-γ-glutamycyclotransferase (γ-GCT) antibody control was similarly purified against recombinant γ-GCT. The use of an unrelated antibody as a control allows the inclusion of non-crossreacting immunoglobulins in the experiments. This is not possible if pre immune serum is used as a control. Purified antibodies were stored at -20°C.

Immunoprecipitation. Protein A sepharose beads were equilibrated overnight with the anti-SPRY2 antibody (2 μg/ml) or with the commercially available 34C antibody (0.05 μg/ml) (Abcam Cambridge, MA USA) or with no antibody. All procedures were performed at 4°C. The beads were washed three times with 500 μl of 20 mM NaPIPES pH 7.4 and incubated with 40 ng of purified RyR1 (80 μl of 25 μg/ml, in 20 mM NaPIPES pH 7.4 plus a protease inhibitor cocktail (Roche) including Calpain I, Calpain II (1.25 μl per 5 ml buffer); Benz, Pepstatin A, Leupeptin, AEBSF, A protinin (1 μl per 1 ml buffer)) for 4 h. The beads were then spun down for 10 s and washed three times with 500 μl of 20 mM NaPIPES pH 7.4 + protease inhibitors. For electrophoresis, the beads were equilibrated with 20 μl of sample buffer for 10 min at 60°C. The supernatant following centrifugation was run on a 4–15% 15-well BioRad precast gel at 200 V for ~40 min under denaturing conditions. The samples were blotted onto nitrocellulose transfer membrane at 125V for ~1½ hours in 37 mM Tris, 140 mM glycine, 20% methanol, blocked for 1 h at room temperature in 5% skim milk in PBS, washed and incubated with primary antibody (34C anti-RyR1 antibody) 1:5,000 in TPBS at 4°C, then washed and incubated with secondary anti-mouse antibody conjugated to HRP 1:5,000 in TPBS for 2 h at room temperature.

The efficacy of the anti-SPRY2 antibody in immunoprecipitating RyR1 was compared with the efficacy of a widely used and commercially available anti-RyR antibody (34C; Abcam Cambridge, MA USA) (**Fig. 2C**). In the experiment shown in **Figure 2D**, the anti-SPRY antibody was incubated with Sepharaose

A beads at a concentration of 2 μg/ml immunoprecipitated the purified RyR1 with 36% of the efficiency (**Fig. 2D**) of the 34C antibody incubated with beads at a concentration of 0.05 μg/ml. Therefore, the 34C antibody was ~118 times more efficient at pulling down purified RyR than the anti-SPRY antibody. It is worth noting that while a similar increased efficacy in RyR1 labeling for 34C was also observed in western Blot experiments, the two antibodies exhibited a similar efficacy in dot blot experiments (Professor Montserrat Samso-personal communication). These results indicate that SPRY antibody binding is strongly dependent on the functionally competent native conformation of the protein, which is maintained in lipid bilayer experiments.

Spectrofluorimetry. Equilibrium dissociation constants for SPRY2 binding to the ASI peptides were determined with a Perkin-Elmer LS 50B6 Spectrofluorimeter using changes in the intrinsic fluorescence in the 203 residue recombinant SPRY2 domain (S^{1085}-V^{1208}, containing two tryptophan residues) in 50 mM sodium phosphate (pH 8) and 300 mM NaCl buffer at 25°C, when aliquots of peptide were added. Excitation was at 280 nm and fluorescence emission monitored at 340 nm. Data, was corrected for dilution effects and for intrinsic peptide fluorescence, and fitted with nonlinear regression using GraphPad Prism software. For analysis, fluorescence (Y) at quencher concentrations (X) were fitted with equation 1 where F_o is the initial fluorescence of the SPRY2 domain without quencher, F_s is the final SPRY2 domain fluorescence with quencher, E_o is the concentration of SPRY2 and K_d is the dissociation constant.[35]

$$Y = F_o - \frac{F_o - F_s}{2E_o}\left(E_o + X + K_d - \sqrt{(E_o + X + K_d)^2 - 4E_oX}\right) \quad \text{(Eqn. 1)}$$

Expression and isolation of ASI(-)RyR1 WT and ASI(-)RyR1 EDE. HEK293 cells were grown in MEM (Minimal Essential Medium) with 10% FCS, at 37°C, 5% CO_2 in T175 culture flasks. The day before transfection, cells were plated out at 50% confluence and the medium was changed 3 hours before transfection. Cells were transfected with a mammalian expression vector (pCIneo) encoding either ASI(-)RyR1 WT or ASI(-)RyR1 EDE (80 μg DNA per flask) using the calcium phosphate precipitation method. Cells were incubated at 37°C for 24 h before the medium was changed and for another 24 hours before they were harvested. For homogenization and solubilization of the recombinant RyR1 constructs, the cell pellet was resuspended in 3 ml of ice-cold Hypotonic Buffer (1 mM EDTA 10 mM Hepes, pH 7.4) containing protease inhibitor cocktail (Roche). The resuspended cells were homogenized once with a French Press (Thermo Scientific) at 1,000 psi. The homogenate was then centrifuged at 3,000 g for 10 min at 4°C. Solubilization buffer (3.75 ml of 33 mM Pipes pH 7.2, 266 μM EDTA, 1.33 M NaCl, 287 μM DTT, 3.33%/1.67% CHAPS/PC) was added to the supernatant and carefully mixed in a tissue grinder with 15 strokes and incubated on ice for 30 min. The mixture was then centrifuged at 163,200 g for 45 min. Then the supernatant was aliquoted and stored at -80°C until further use.

Expression and intracellular Ca^{2+} measurements in HEK293 cells. HEK293 cells were grown in DMEM/10% FBS at 37°C, 5% CO_2 and transfected with full-length ASI(-) WT RyR1 or EDE mutant cDNA using lipofectamine at 70% cell confluence and a DNA:lipofectamine ratio of 1:2.5 (12 μg DNA/10 cm culture dish). This transfection protocol resulted in an ~70% transfection efficiency. Ca^{2+} measurements were carried out 36–48 h after transfection. Following loading with 5 μM Fura-2 in Ringer solution for 45 min at 37°C, cells were alternately excited by 340 and 380 nm (510 nm emission) every 1 s (20 ms exposure per wavelength and 1 x 1 binning) using a monochrometer-based illumination system and captured using a high speed, digital QE CCD camera (TILL Photonics, Pleasanton, CA USA). Thirty seconds of different concentrations of 4-chloro-m-cresol (4-CMC) were applied using a local profusion system, with a 50 s of washout with control Ringer solution between applications. Only 2–3 concentrations of 4-CMC were applied to any given cell in order to minimize 4-CMC toxicity. Fura-2 ratios ($R = F_{340}/F_{380}$) were generated offline and used to determine peak 4-CMC responses ($\Delta R = R_{peak} - R_{base}$). Concentration-response curves were generated by combining peak responses to 1, 5, 10, 30, 50, 100, 300, 1,000 μM 4-CMC and then the results fitted using a standard Hill equation.

Preparation and nuclear cDNA injections of RyR1-null myotubes. Primary cultures and nuclear cDNA injections of myotubes from RyR1-null mice were performed as described previously.[20] Briefly, cDNAs encoding either wild-type ASI(-)RyR1 (ASI(-)RyR1 WT), E1108A/D1112A double mutant (ASI(-)RyR1 ED), or E1108A/D1112A/E1114A triple mutant (ASI(-)RyR1 EDE) were microinjected into nuclei of individual myotubes at 0.5 μg/μl. Co-injection of CD8 cDNA (0.1 μg/μl) was used to identify expressing myotubes by incubation with CD8 antibody-coated beads.

Intracellular Ca^{2+} measurements in myotubes. Myotubes expressing wild-type or ASI mutant RyR1s were loaded for 1 h at 37°C with 6 μM Indo-1 AM (TEFLABS, Austin, TX USA), in a Ringer's solution containing: 146 mM NaCl, 5 mM KCl, 2 mM $CaCl_2$, 1 mM $MgCl_2$, 10 mM HEPES, pH 7.4 Intracellular Ca^{2+} transients were measured as described previously.[32] Indo-1 loaded myotubes were excited at 350 nm and fluorescence emission measured at 405 nm and 485 nm. A series of stimuli were sequentially applied to myotubes including electrical stimulation (80 V, 5 ms) at a frequency of 0.1 Hz, followed by 30 s of 30 mM caffeine and 500 μM 4-CMC, with a 30 s washout in between. All stimulations were delivered locally either by glass pipette electrode or by local perfusion. Results were presented as the ratio of fluorescence at 405 nm and 485 nm (F_{405}/F_{485}).

Voltage clamp measurements. Voltage-gated L-type Ca^{2+} currents (L-currents) and intracellular Ca^{2+} transients were simultaneously recorded from WT and mutant ASI(-)RyR1-expressing myotubes using the whole-cell patch clamp technique.[36] For these experiments, the external solution contained: 145 mM TEA-Cl, 10 mM $CaCl_2$, 10 mM HEPES, pH 7.4 and the pipette internal solution contained: 145 mM Cs-aspartate, 0.1 mM EGTA, 1.2 mM $MgCl_2$, 0.2 mM K_5-Fluo-4, 5 mM Mg-ATP, 10 mM HEPES, pH 7.4. Cell capacitance was determined by integration

of the capacity transient resulting from a +10 mV pulse applied from the holding potential (-80 mV) and was used to normalize Ca^{2+} currents (pA/pF) from different myotubes. Peak L-current density (pA/pF) was plotted as a function of membrane potential and fitted according to:

$$I_{Ca} = G_{max} \bullet (V_m - V_{rev})/(1 + \exp[(V_{G1/2} - V_m)/k_G]) \quad \text{(Eqn. 2)}$$

where G_{max} is the maximum L-channel conductance, V_m is the test potential, V_{rev} is the reversal potential, $V_{G1/2}$ is the voltage for half-maximal activation of G_{max} and k_G is a slope factor. Relative changes in intracellular Ca^{2+} in patch clamp experiments were simultaneously recorded during each test pulse and are reported as ΔF/F, where F is the baseline fluorescence immediately prior to depolarization and ΔF is the fluorescence change from baseline. Fluorescence amplitudes at the end of each test pulse were plotted as a function of membrane potential and fitted according to:

$$\Delta F/F = (\Delta F/F)_{max}/\{1 + \exp[(V_{F1/2} - V_m)/k_F]\} \quad \text{(Eqn. 3)}$$

where $(\Delta F/F)_{max}$ is the maximal fluorescence change, V_m is the test potential, $V_{F1/2}$ is the voltage for half activation of $(\Delta F/F)_{max}$ and k_F is a slope factor.

SR vesicle isolation, single channel recording and analysis. Rabbit skeletal SR vesicles were isolated and incorporated in lipid bilayers[37-39] using a cis (cytoplasmic) solution containing: 230 mM $CsCH_3O_3S$, 20 mM CsCl, 1.0 mM $CaCl_2$, 10 mM TES and 500 mM mannitol (pH 7.4, with CsOH) and a trans (luminal) solution containing 30 mM $CsCH_3O_3S$, 20 mM CsCl, 1 mM $CaCl_2$ and 10 mM TES (pH 7.4).[38,39] Following RyR incorporation, the cis solution was replaced with a similar solution, lacking mannitol and having 10 μM free Ca^{2+} (buffered with BAPTA, adjusted using a Ca^{2+} electrode). 200 mM $CsCH_3O_3S$ was added to the trans solution to achieve symmetrical 250 mM Cs^+. Bilayer potential, $V_{cis} - V_{trans}$, was switched between -40 and +40 mV every 30 s. Channel activity under each condition was analyzed over 60 to 120 s using the program Channel 2 (developed by PW Gage and M Smith, JCSMR). Threshold levels for channel opening were set to exclude baseline noise at ~20% of the maximum single channel conductance. A curve describing the peptide concentration - dependence of relative P_o (^RP_o) was constructed using the sum of Hill equations for activation and inhibition:[40]

$$^RP_o = {}^RP_{o\min} + ({}^RP_{o\max} - {}^RP_{o\min})\ (1/[1 + (AC_{50}/[F])\text{^}Ha]) \quad \text{(Eqn. 4, activation)}$$

$$^RP_o = {}^RP_{o\min} + ({}^RP_{o\max} - {}^RP_{o\min})\ (1/[1 + ([F]/IC_{50})\text{^}Hi]) \quad \text{(Eqn. 5, inhibition)}$$

$^RP_{o\max}$ and $^RP_{o\min}$ are the relative P_o of the minimally and maximally activated channel, AC_{50} and IC_{50} are the **F** [peptide] for half-maximal activation and inhibition respectively, and Ha and Hi are the corresponding Hill coefficients. Curves were fitted to the data using the least squares method.

Statistics. Average data are given as mean ±SEM. Statistical significance was evaluated using paired or unpaired Student's t-test as appropriate or ANOVA. Numbers of observations (n) are given in tables and figure legends. For data shown in **Figures 1 and 2**, either one peptide concentration was tested in each experiment (**Fig. 1**) or antibodies not always added sequentially at 1 μg/ml then 5 μg/ml (**Fig. 2**: in five cases 1 μg/ml was followed by 5 μg/ml, in a further five cases the bilayer broke after exposure to 1 μg/ml, before exposure to 5 μg/ml antibody). Thus there were separate sets of control data for each concentration of F peptide or antibody, necessitating the use of ANOVA and post-hoc Mahalanobis tests. To reduce effects of variability in control parameters (P_oC, T_oC, T_cC), and to evaluate parameters after F peptide (P_oF, T_oF, T_cF) or antibody (P_oA, T_oA, T_cA) addition, data were expressed as the difference between $\log_{10} XC$ and $\log_{10} XF$ (or $\log_{10} XA$) for each channel (e.g., $\log_{10}P_oF - \log_{10}P_oC$). The difference from control was assessed with a paired t-test applied to $\log_{10}P_oC$ and $\log_{10}P_oF$. The difference between each concentration was assessed using ANOVA on $\log_{10}P_oC - \log_{10}P_oF$ at each concentration with the post-hoc multidimensional Mahalanobis test. A p value of <0.05 was considered significant.

Conclusions

We demonstrate that the SPRY2 domain of RyR1, and specifically the **F** loop domain, contributes to RyR1 ion channel gating by the **F** loop interacting with a regulatory site on the RyR tetramer. We also show that the SPRY2 domain and its **F** loop bind to the ASI/basic region of the RyR via an electrostatic interaction mediated by specific acidic residues in the **F** loop with a series of basic residues in the ASI/basic region, as well as additional structural constraints within the ASI/basic α-helix. The results indicate that the functional consequence of the **F** loop interdomain interaction with the ASI/basic region may be interrupted by the influence of conditions specific to the intact cells on RyR1, in a similar manner to how DHPR interactions with RyR1 disrupt imperatoxin A sensitivity. The results also indicate that the previously identified impact of the ASI/basic region on EC coupling is not mediated by an interaction with the SPRY2 domain **F** loop.

Acknowledgements

The authors are grateful to S. Pace and J. Stivala for SR vesicle preparation, to M. Coggan for assistance with SPRY2 domain expression and purification, and L. Groom for generating the full-length RyR1 SPRY2 **F** loop mutants. We also thank Dr. P.D. Allen for providing access to the RyR1-null mice used in this study. The work was supported by the NHMRC (#471462 to Angela F. Dulhunty), the NIH (AR44657 to Robert T. Dirksen) and the Academia Dei Lincei Fund (Lan Wei).

References

1. Tanabe T, Beam KG, Adams BA, Niidome T, Numa S. Regions of the skeletal muscle dihydropyridine receptor critical for excitation-contraction coupling. Nature 1990; 346:567-9.
2. Ponting C, Schultz J, Bork P. SPRY domains in ryanodine receptors (Ca^{2+}-release channels). Trends Biochem Sci 1997; 22:193-4.
3. Tae H, Casarotto MG, Dulhunty AF. Ubiquitous SPRY domains and their role in the skeletal type ryanodine receptor. Eur Biophys J 2009.
4. Sheridan DC, Takekura H, Franzini-Armstrong C, Beam KG, Allen PD, Perez CF. Bidirectional signaling between calcium channels of skeletal muscle requires multiple direct and indirect interactions. Proc Natl Acad Sci USA 2006; 103:19760-5.
5. Altafaj X, Cheng W, Esteve E, Urbani J, Grunwald D, Sabatier JM, et al. Maurocalcine and domain A of the II-III loop of the dihydropyridine receptor $Ca_v1.1$ subunit share common binding sites on the skeletal ryanodine receptor. J Biol Chem 2005; 280:4013-6.
6. Leong P, MacLennan DH. A 37-amino acid sequence in the skeletal muscle ryanodine receptor interacts with the cytoplasmic loop between domains II and III in the skeletal muscle dihydropyridine receptor. J Biol Chem 1998; 273:7791-4.
7. Nabhani T, Zhu X, Simeoni I, Sorrentino V, Valdivia HH, Garcia J. Imperatoxin a enhances Ca^{2+} release in developing skeletal muscle containing ryanodine receptor type 3. Biophys J 2002; 82:1319-28.
8. Chen L, Esteve E, Sabatier JM, Ronjat M, De Waard M, Allen PD, et al. Maurocalcine and peptide A stabilize distinct subconductance states of ryanodine receptor type 1, revealing a proportional gating mechanism. J Biol Chem 2003; 278:16095-106.
9. Bannister ML, Williams AJ, Sitsapesan R. Removal of clustered positive charge from dihydropyridine receptor II-III loop peptide augments activation of ryanodine receptors. Biochem Biophys Res Commun 2004; 314:667-74.
10. Schneider MF, Rodney GG. Peptide and protein modulation of local Ca^{2+} release events in permeabilized skeletal muscle fibers. Biol Res 2004; 37:613-6.
11. Pouvreau S, Csernoch L, Allard B, Sabatier JM, De Waard M, Ronjat M, et al. Transient loss of voltage control of Ca^{2+} release in the presence of maurocalcine in skeletal muscle. Biophys J 2006; 91:2206-15.
12. Altschafl BA, Beutner G, Sharma VK, Sheu SS, Valdivia HH. The mitochondrial ryanodine receptor in rat heart: a pharmaco-kinetic profile. Biochim Biophys Acta 2007; 1768:1784-95.
13. Cui Y, Tae HS, Norris NC, Karunasekara Y, Pouliquin P, Board PG, et al. A dihydropyridine receptor alpha1s loop region critical for skeletal muscle contraction is intrinsically unstructured and binds to a SPRY domain of the type 1 ryanodine receptor. Int J Biochem Cell Biol 2009; 41:677-86.
14. Tae HS, Norris NC, Cui Y, Karunasekara Y, Board PG, Dulhunty AF, et al. Molecular recognition of the disordered dihydropyridine receptor II-III loop by a conserved spry domain of the type 1 ryanodine receptor. Clin Exp Pharmacol Physiol 2009; 36:346-9.
15. Nakai J, Tanabe T, Konno T, Adams B, Beam KG. Localization in the II-III loop of the dihydropyridine receptor of a sequence critical for excitation-contraction coupling. J Biol Chem 1998; 273:24983-6.
16. Grabner M, Dirksen RT, Suda N, Beam KG. The II–III loop of the skeletal muscle dihydropyridine receptor is responsible for the Bi-directional coupling with the ryanodine receptor. J Biol Chem 1999; 274:21913-9.
17. Zorzato F, Fujii J, Otsu K, Phillips M, Green NM, Lai FA, et al. Molecular cloning of cDNA encoding human and rabbit forms of the Ca^{2+} release channel (ryanodine receptor) of skeletal muscle sarcoplasmic reticulum. J Biol Chem 1990; 265:2244-56.
18. Zorzato F, Sacchetto R, Margreth A. Identification of two ryanodine receptor transcripts in neonatal, slow- and fast-twitch rabbit skeletal muscles. Biochem Biophys Res Commun 1994; 203:1725-30.
19. Futatsugi A, Kuwajima G, Mikoshiba K. Tissue-specific and developmentally regulated alternative splicing in mouse skeletal muscle ryanodine receptor mRNA. Biochem J 1995; 305:373-8.
20. Kimura T, Nakamori M, Lueck JD, Pouliquin P, Aoike F, Fujimura H, et al. Altered mRNA splicing of the skeletal muscle ryanodine receptor and sarcoplasmic/endoplasmic reticulum Ca^{2+}-ATPase in myotonic dystrophy type 1. Hum Mol Genet 2005; 14:2189-200.
21. Kimura T, Pace SM, Wei L, Beard NA, Dirksen RT, Dulhunty AF. A variably spliced region in the type 1 ryanodine receptor may participate in an inter-domain interaction. Biochem J 2007; 401:317-24.
22. Kimura T, Lueck JD, Harvey PJ, Pace SM, Ikemoto N, Casarotto MG, et al. Alternative splicing of RyR1 alters the efficacy of skeletal EC coupling. Cell Calcium 2009; 45:264-74.
23. Cheng W, Altafaj X, Ronjat M, Coronado R. Interaction between the dihydropyridine receptor Ca^{2+} channel beta-subunit and ryanodine receptor type 1 strengthens excitation-contraction coupling. Proc Natl Acad Sci USA 2005; 102:19225-30.
24. Samso M, Trujillo R, Gurrola GB, Valdivia HH, Wagenknecht T. Three-dimensional location of the imperatoxin A binding site on the ryanodine receptor. J Cell Biol 1999; 146:493-9.
25. Samso M, Wagenknecht T. Apocalmodulin and Ca^{2+}-calmodulin bind to neighboring locations on the ryanodine receptor. J Biol Chem 2002; 277:1349-53.
26. Copello JA, Barg S, Onoue H, Fleischer S. Heterogeneity of Ca^{2+} gating of skeletal muscle and cardiac ryanodine receptors. Biophys J 1997; 73:141-56.
27. Wei L, Gallant EM, Dulhunty AF, Beard NA. Junctin and triadin each activate skeletal ryanodine receptors but junctin alone mediates functional interactions with calsequestrin. Int J Biochem Cell Biol 2009; 41:2214-24.
28. Casarotto MG, Green D, Pace S, Young J, Dulhunty AF. Activating the ryanodine receptor with dihydropyridine receptor II-III loop segments: size and charge do matter. Front Biosci 2004; 9:2860-72.
29. Casarotto MG, Green D, Pace SM, Curtis SM, Dulhunty AF. Structural determinants for activation or inhibition of ryanodine receptors by basic residues in the dihydropyridine receptor II–III loop. Biophys J 2001; 80:2715-26.
30. Yamamoto T, El-Hayek R, Ikemoto N. Postulated role of interdomain interaction within the ryanodine receptor in Ca^{2+} channel regulation. J Biol Chem 2000; 275:11618-25.
31. Kobayashi S, Yamamoto T, Parness J, Ikemoto N. Antibody probe study of Ca^{2+} channel regulation by interdomain interaction within the ryanodine receptor. Biochem J 2004; 380:561-9.
32. Goonasekera SA, Beard NA, Groom L, Kimura T, Lyfenko AD, Rosenfeld A, et al. Triadin binding to the C-terminal luminal loop of the ryanodine receptor is important for skeletal muscle excitation contraction coupling. J Gen Physiol 2007; 130:365-78.
33. Dulhunty AF, Haarmann CS, Green D, Laver DR, Board PG, Casarotto MG. Interactions between dihydropyridine receptors and ryanodine receptors in striated muscle. Prog Biophys Mol Biol 2002; 79:45-75.
34. Board PG, Webb GC. Isolation of a cDNA clone and localization of human glutathione S-transferase 2 genes to chromosome band 6p12. Proc Natl Acad Sci USA 1987; 84:2377-81.
35. Birdsall B, King RW, Wheeler MR, Lewis CA Jr, Goode SR, Dunlap RB, et al. Correction for light absorption in fluorescence studies of protein-ligand interactions. Anal Biochem 1983; 132:353-61.
36. Dirksen RT, Avila G. Distinct effects on Ca^{2+} handling caused by malignant hyperthermia and central core disease mutations in RyR1. Biophys J 2004; 87:3193-204.
37. Saito A, Seiler S, Chu A, Fleischer S. Preparation and morphology of sarcoplasmic reticulum terminal cisternae from rabbit skeletal muscle. J Cell Biol 1984; 99:875-85.
38. Beard NA, Wei L, Cheung SN, Kimura T, Varsanyi M, Dulhunty AF. Phosphorylation of skeletal muscle calsequestrin enhances its Ca^{2+} binding capacity and promotes its association with junctin. Cell Calcium 2008; 44:363-73.
39. Wei L, Varsanyi M, Dulhunty AF, Beard NA. The conformation of calsequestrin determines its ability to regulate skeletal ryanodine receptors. Biophys J 2006; 91:1288-301.
40. Laver DR. Ca^{2+} stores regulate ryanodine receptor Ca^{2+} release channels via luminal and cytosolic Ca^{2+} sites. Biophys J 2007; 92:3541-55.